Cyclic thermogravimetry of TBC systems

Aurélie Vande Put , Daniel Monceau and Djar Oquab

CIRIMAT, ENSIACET, 118 route de Narbonne, 31077 Toulouse, Cedex 4, France

Abstract

The previously developed cyclic thermogravimetry analysis (CTGA) method is applied to the cyclic oxidation at 1100 °C of ZrO_2–Y_2O_3/NiPtAl or NiCoCrAlYTa/single crystal nickel-base AM3 superalloy TBC systems. Cyclic thermogravimetry with fast heating and cooling and high accuracy in mass measurement allows to measure oxidation kinetics of the bond coating and also to detect and quantify the occurrence of the top coating cracking and spalling. The resulting data could be used later on, for time of life modelling of TBC systems.

Keywords: TBC; Thermogravimetry; CTGA; Cyclic oxidation

1. Introduction

In previous work, a quantitative analysis of continuous cyclic thermogravimetry (CTGA) was developed [1] and applied to the high temperature cyclic oxidation of NiAl [1] and [2], NiCoCrAlYTa coated or uncoated MC2 superalloy [3], NiPtAlHf alloy [4] and FeNiCr austenitic steels [5]. This technique allows to follow the Net Mass Change (NMC) but also the Gross Mass Gain, the oxide scale thickness, the oxidation kinetics, the amount of spalling and the mass of consumed metal as a function of cycle number. Then, the cyclic oxidation test becomes an automatic test, which produces a quantitative description of cyclic oxidation kinetics in terms of a combination of the isothermal oxidation kinetics (parameter "k_p") and of spalling kinetics (parameter "P"). "k_p" and "P" can be constant or may vary with time and can be plotted on performance maps [3] and [6]. CTGA is an experimental tool complementary to cyclic oxidation kinetics models [6], [7], [8] and [9].

CTGA was used for specific high temperature applications for which alloying element consumption controls lifetime [1], [2], [3], [4] and [5]. In the case of Thermal Barrier Coating (TBC) systems, the problem is somewhat different as no, or negligible, top coating spalling is allowed. In fact, once spalling is detected, damage generally develops fast enough so that the end of life can be identified with a fair amount of top coating spalling (20 or 30%). The question of

life prediction is then linked to the occurrence of the first spall rather than to the quantification of the spalling kinetics. That's why most TBC life models deal with the mechanical description of a thermally cycled ceramic/metal composite [10]. The problem is complex because the system changes with time (zirconia sintering, alumina growth and creep, composition changes and phase transformations of bond coating, interfacial morphology, chemistry and adhesion evolutions). This lifetime modelling requires many physical data and precise experiments to check assumptions.

The present paper gives preliminary results of CTGA applied to TBC systems. The ability of this technique to obtain some of the data requested by the models is tested. These data include the isothermal oxidation kinetics of bond coatings (BC) under the zirconia top coating, the occurrence of cracking or top coating spalling, the temperature at which spalling occurs, the amount of spalling and the Thermally Grown Oxide (TGO) thickness at which the spalling occurs.

2. Materials and experimental procedures

AM3 single crystal nickel-base superalloy was used as substrate in TBC systems. Two BC were investigated: NiCoCrAlYTa and NiPtAl. The first was vacuum plasma sprayed (VPS). Concerning the modified nickel aluminide coating, Pt was deposited through an electrolytic process followed by a vapor phase aluminization (APVS). AM3 single crystal and NiCoCrAlYTa BC compositions are given in Table 1. The 50 μm thick Pt-modified aluminide coating is composed of about 35 at.% (15 wt.%) of Al and more than 10 at.% (32 wt.%) of Pt (EDS measurements). Besides, several at.% of Cr, Co and Ti can be found up to the external surface of the BC. The top coating made of zirconia with 7 wt.% yttria was deposited by electron beam physical vapor deposition (EBPVD) on grit blasted and preoxidized BC (3 h at 1000 °C in air at 0.5 mbar). Because of process requirement, a stem in Hastelloy X is welded to AM3 disc. The overall surface of the stem is also covered by the bond coating and zirconia except its extremity which is covered by a NiCoCrAlYTa bond coating alone. More details about these systems can be found in [11].

Table 1.

AM3 single crystal and NiCoCrAlYTa bond coating composition

		Al	Ta	Cr	Ti	Mo	Co	W	Ni
AM3	wt.%	6.0	4.0	8.0	2.0	2.0	6.0	5.0	Balance
	at.%	13	1.3	8.9	2.4	1.2	5.9	1.6	Balance
NiCoCrAlYTa	wt.%	8.6	3.9	22	–	–	23	–	Balance
(AMDRY 997)	at.%	17	1.1	21	–	–	21	–	Balance

Before being thermally cycled, samples were oxidized 20 h under flowing dry O_2 at 1100 °C or 900 °C in a thermobalance to measure with precision the initial oxidation rates. Cyclic oxidation tests were performed using two systems: SETARAM TAG24S thermobalance and CTGA thermobalance. Thanks to its symmetrical furnace arrangement, the SETARAM TAG24S offers an excellent accuracy (about 1 μg) with limited drift and buoyancy effects. The difference between the mass of the TBC system and the mass of an inert alumina reference sample placed in the symmetrical furnace was recorded continuously during thermal cycling, as detailed in [1]. The CTGA thermobalance was developed and patented in the laboratory [12]. This apparatus combines a lamps furnace with 5 balances measuring the mass changes of 5 independent samples in a controlled atmosphere (Fig. 1).

Fig. 1. CTGA thermobalance.

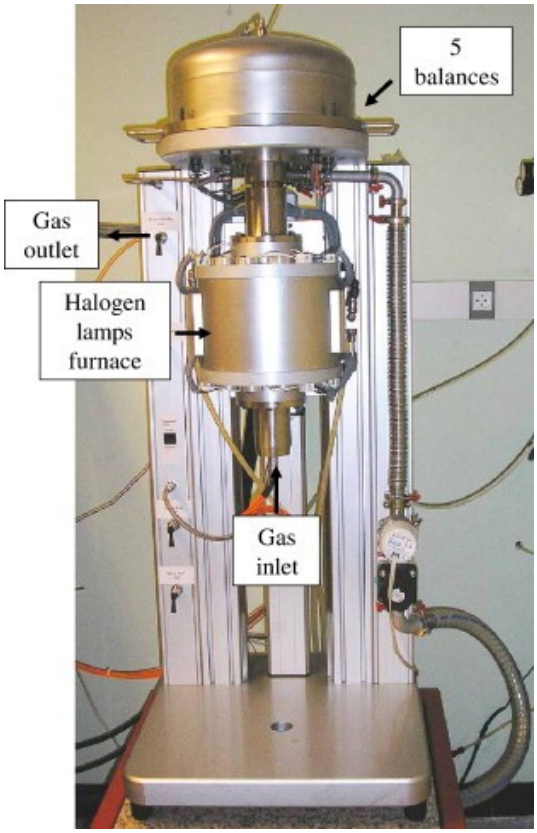

Thermal cycles realized during this study are presented in Table 2. One cycle consists in heating at 60 °C/min (TAG24S) or 140 °C/min (CTGA) up to 1100 °C, a high temperature dwell of 1 h at 1100 °C followed by cooling down to 200 °C at an initial rate of 90 °C/min (TAG24S) or 300 °C/min (CTGA) and a 15 min hold time at 200 °C. Those tests were realized under flowing synthetic air (0.2–1 l/h for each sample). The two types of TBC systems (NiPtAl BC and NiCoCrAlYTa BC), previously oxidized 20 h at 900 °C in O_2, were tested in the SETARAM TAG24S . The same TBC systems, except that they were first oxidized 20 h at 1100 °C in O_2, were tested in the new CTGA thermobalance (Table 3). In the CTGA apparatus, 5 samples can be oxidized simultaneously. The 2 TBC samples were cycled at the same time as an AM3 disc, a massive porous zirconia sample used as a reference, and a TBC sample in which a hole was drilled to place a control S-type thermocouple. Just 3–5 mm below the 5 samples, 5 additional S-type thermocouples with FeCrAlY caps were used for the furnace regulation. This furnace includes 10 halogen lamps divided in 5 groups (2 lamps for each sample) with 5 independent temperature regulations.

Table 2.

Thermal cycles for CTGA thermobalance and TAG24S thermobalance

	Low $T°$	High $T°$	Heating time[a]	Hot dwell time	Cooling time[a]	Cold dwell time
	°C	°C	s	min	s	min
TAG24S	200	1100	867	60	1133	15
CTGA	200	1100	370	60	1906	15

[a] According to COTEST [European RTD Project No. GRD1-2001-40037M-T, 2005].

Table 3.

Oxidation kinetics of TBC systems and bond coatings

		k_p	Cycles	Apparatus
		10^{-7} mg^2/(cm^4 · s)		
Isothermal oxidation (20 h, O_2, 1100 °C)				
TBC30	ZrO_2/NiPtAl-preoxidized	9.5	–	TAG24S
Cyclic oxidation (syn. air, 1100 °C)				
TBC30	ZrO_2/NiPtAl-preoxidized + 20 h − 1100 °C	7.8	1–90	CTGA
		9.6	1–115	
TBC29	ZrO_2/NiPtAl-preoxidized + 20 h − 900 °C	11.7	1–20	TAG24S
		8.8	1–90	
		10.7	1–204	
		2.5	210–290	
		2.9	305–376	
		2.5	392–402	
		0.5	461–480	
TBC47	ZrO_2/NiCoCrAlYTa-preoxidized + 20 h − 900 °C	10.2	1–20	

		k_p	Cycles	Apparatus
		10^{-7} mg^2/(cm^4 · s)		
		7.2	1–90	
		2.3	93–104	
		2.0	163–186	
		2.8	240–260	

3. Continuous cyclic thermogravimetry measurements analysis (CTGA)

This paragraph explains how thermogravimetry under cyclic conditions is used to determine independently the mass gain due to oxidation and the mass loss due to spalling. Fig. 2 shows the Net Mass Change for the TBC samples during cyclic oxidation. Both oxidation and spalling can be clearly observed.

Fig. 2. Net Mass Change versus cycle number for TBC systems (1 h cycles at 1100 °C in flowing dry air). S = thermal cycling was stopped so temperature decreased below 200 °C. O = the furnace was open. Then, temperature decreased below 200 °C and the environment changed.

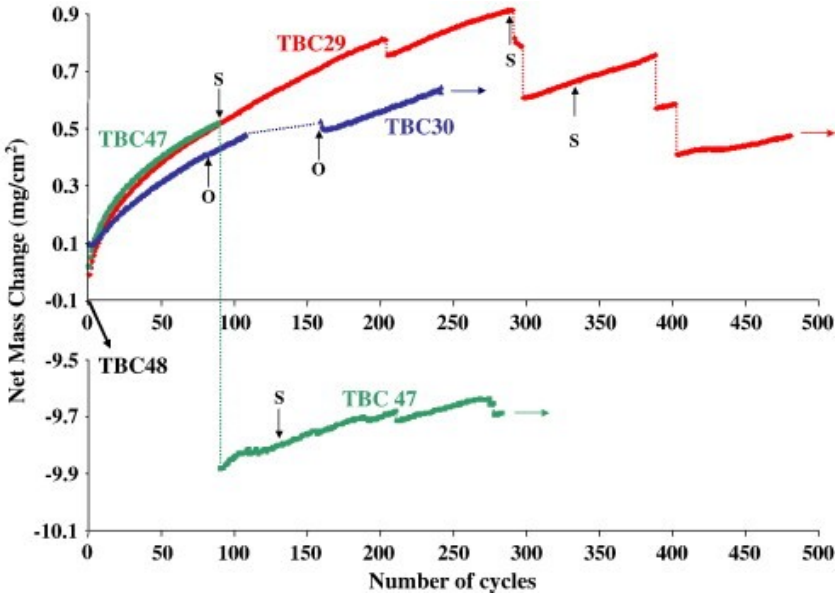

At 1100 °C, the oxidation kinetics of BCs are low enough so that very long experiments or very precise measurements are necessary. For a pure nickel-base alumina former, k_p at 1100 °C is below 10^{-6} $mg^2/cm^4/s$. Then, the expected mass gain of a non-preoxidized sample is about 60 µg/cm2 during the first cycle, 3 $µg/cm^2$ during the 100th cycle and less than 1 $µg/cm^2$ during the 1000th cycle. During this study, it was shown that the Pt wire which is used to hang the specimen is losing weight because of evaporation. With the massive zirconia reference sample, the rate of mass loss due to evaporation was measured over 300 cycles and corresponds to a constant mass loss rate of 3.3 $µg/cm^2$/cycle for a TBC sample. It appears that this value cannot be neglected in front of the mass gain due to oxidation so the NMC signal was corrected to take into account this phenomenon. For the SETARAM TAG24S thermobalance, Pt evaporation is not a problem because of the symmetrical arrangement. Fig. 3 is an enlargement of Fig. 2 during cycles 3 and 4 of TBC29. The mass gains due to oxidation during the high temperature dwells can be seen. Between these dwells, the mass varies due to buoyancy and convection. As explained in [1], it is possible to analyze only the mass recorded during high temperature dwells with no effect of buoyancy or convection. Indeed, it can be seen on Fig. 3 that the mass at the end of a high temperature dwell (point A) is equal to the mass at the beginning of the next high temperature dwell (point B). The overall NMC data of Fig. 2 are obtained by selecting the last point of each high temperature dwell. From these data, in cycle ranges without spalling event, k_p can be calculated using the complete parabolic fitting procedure [13]. Results are given in Table 3.

Fig. 3. Temperature and Net Mass Change of TBC29 during cycles 3 and 4.

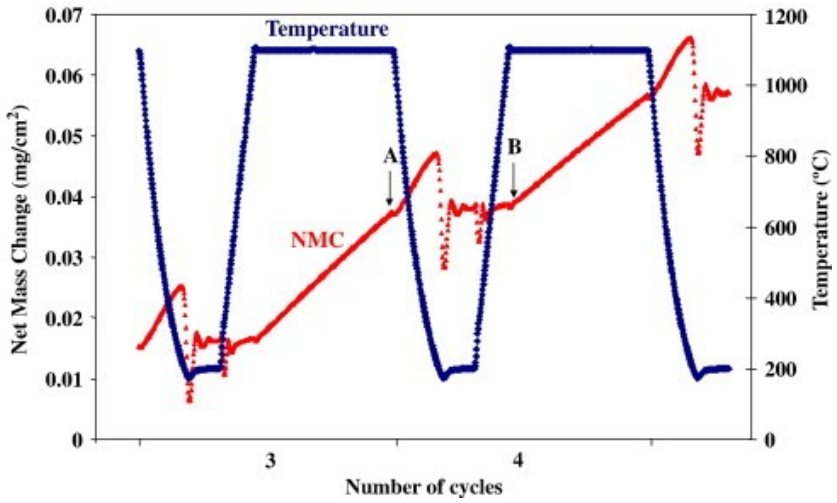

Concerning spalling, both the top coating (TC) and the TGO may spall. The zirconia layer is about 100 µm thick with a density of about 6 g/cm^3. The TGO layer grows up to about 10 µm and has a density of about 4 g/cm^3. Then, the mass loss due to TGO spalling is at maximum 7% of the total mass loss. Most of the time, this proportion is inferior because TGO layer thickness is less than 10 µm or because the system spalls sometimes at the zirconia/alumina interface. Then, thermogravimetry measures the mass of spalled zirconia. TC mass is about 60 mg/cm^2, i.e. more than 3 order of magnitude higher than the mass gain due to oxidation. This means that very small spalls can be detected, i.e. 0.001% of the top coating. Then, thermogravimetry may detect eye-invisible spalling, around cracks for example.

Spalling events are shown on Fig. 4 which is an enlargement of Fig. 2 during cycles 292 and 298 for TBC29. Continuous mass recording allows to determine the mass of the spalls, but also the temperature at which zirconia spalls. In this example, spalling occurs during cooling at cycle 298, but during heating at cycle 292.

Fig. 4. Temperature and Net Mass Change of TBC29 during cycles 292 and 298, detection of spalling events during heating (cycle 292) and cooling (cycle 298).

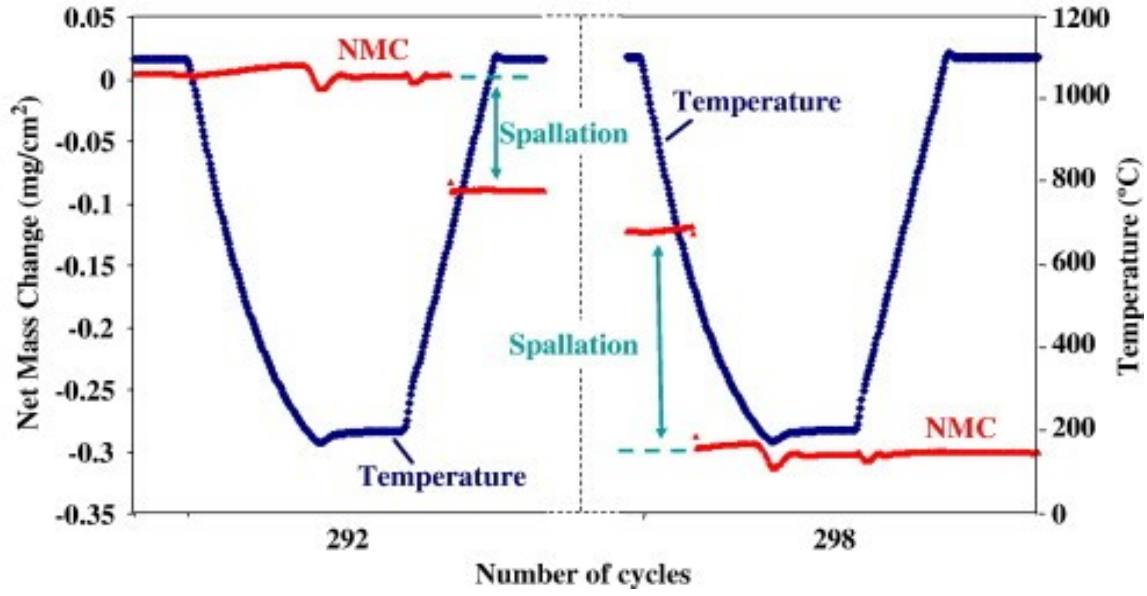

4. Results and discussion

As described previously, 4 TBC systems were submitted to thermal cycling. Similar tests were realized in a high precision SETARAM TAG24S commercial thermobalance and in a new multi-samples CTGA apparatus. Two samples with NiCoCrAlYTa BC (TBC47 and TBC48) and two with NiPtAl BC (TBC29 and TBC30) were tested, one of each kind in each apparatus. Fig. 2 shows the global NMC of 3 of the 4 tested TBC samples. The data for the NiCoCrAlYTa-base system (TBC48) tested in the CTGA apparatus is not available because of a technical reason. Nevertheless, this sample was submitted to 80 cycles at 1100 °C. When the furnace was opened to remove the sample, large parts of the top coating spalled with projections up to 1 m away. From mass measurements before and after the test, the proportion of the spalled top coating was estimated to be around 55%. At the first opening of the CTGA apparatus furnace, the NiPtAl-base system (TBC30) did not suffer from spalling. This sample was left in the apparatus and was cycled up to 481 cycles (still cycling) (Fig. 2).

Table 3 gives the k_p calculated from isothermal and cyclic oxidation data. They show that oxidation kinetics of NiCoCrAlYTa BC is similar to NiPtAl. Comparing NiPtAl-base system (TBC29) with NiCoCrAlYTa-base system (TBC47) in Table 3, the initial parabolic constant is around $7–12 \cdot 10^{-7}$ before decreasing down to about $2 \cdot 10^{-7}$ mg cm^{-4} s^{-1} after few hundreds of cycles, for both systems. This is explained by the growth of a pure alumina layer on NiPtAl as well as on NiCoCrAlYTa. A second observation is that, for NiPtAl, the parabolic constants calculated from the mass change under cyclic oxidation (TBC29 and TBC30) are very closed to the parabolic constants calculated from the first 20 h of isothermal oxidation under O_2 (TBC30). After longer times and between small zirconia spalling events, kp is decreasing for both NiCoCrAlYTa and NiPtAl BCs (TBC29 and TBC47). This may be due to TGO grain growth decreasing grain boundary diffusion. It also confirms that up to the current number of cycles, the TGO diffusion barrier was not damaged.

Fig. 2 and Fig. 4 show the occurrence of spalling events. The mass losses associated with these events are gathered in Table 4. In this table, it can be seen that 8 spalling events were detected for TBC29 (NiPtAl) and 13 for TBC47 (NiCoCrAlYTa). Most of these spalling events correspond to very small percentages of the total mass of zirconia top coating (0.01–0.3%), except for one large spalling which occurred after 90 cycles for TBC47 (Fig. 2, Table 4). This spalling corresponds to 16% of the top coating and occurred after overnight thermobalance stop due to power failure (which lead to a temperature decrease down to room temperature). The sample remained in the close furnace under synthetic dry air atmosphere. The same stop occurs for TBC29 after 290 cycles without causing any spalling (Fig. 2). As can be seen on Fig. 2, another stop of the cyclic oxidation occurs at cycle 331 (TBC29) and 131 (TBC47). This stop was a return to ambient temperature during a few minutes still under controlled dry atmosphere. It was followed by several small spalling events on cycles 291–298 for TBC29 and no spalling for TBC47. Table 4 also shows the temperature at which the spalling occurs. This temperature is very variable, from 1043 °C to 171 °C. Spalling generally occurs during cooling. But it is remarkable that for 21 spallation events, spalling occurs 4 times during heating and always at high temperature (664 to 1043 °C).

Table 4.

Quantification of spalling for TBC29 and TBC47

Sample ID	Cycle	Δm/S mg/cm^2	Spalls mass[a] %	Cooling/heating	Temperature °C (+/− 5)
TBC29	205	0.052	0.087	C	708
	291	0.002	0.003	C	N.A.
	292	0.094	0.157	H	664
	293	0.012	0.020	C	503
	298	0.178	0.297	C	549
	389	0.186	0.311	C	441
	403	0.175	0.291	C	512
	427	0.005	0.009	C	283
TBC47	91	10.457	17.4	C	N.A.
	111	0.018	0.030	C	372
	117	0.012	0.020	C	194
	123	0.012	0.020	C	277
	132	0.007	0.011	C	N.A.
	157	0.006	0.010	C	967
	157	0.006	0.010	H	755
	189	0.006	0.010	C	936
	191	0.012	0.020	C	218
	211	0.033	0.055	H	1043
	270	0.006	0.010	C	171
	276	0.018	0.030	C	417
	279	0.039	0.065	H	900

[a] % of total mass of zirconia top coat.

Fig. 2 and Table 4 show the higher cyclic oxidation resistance of the NiPtAl-base systems when compared to the NiCoCrAlYTa-base systems. The NiPtAl-base system is not superior in terms of oxidation kinetics (Table 3), but it experiences less spalling in both apparatus. Then, this difference in performance is apparently not due to the simple mechanical effect of TGO thickness, but to a more complex mechanism. This preliminary observation confirms previous cyclic oxidation tests which were performed at 1200 °C in a burner rig on the same batch of samples [11]. Sample TBC48 (NiCoCrAlYTa) was observed in SEM-EDX after 80 cycles at 1100 °C. Fig. 5 shows the decohesion of the TGO/BC interface. This decohesion occurs for a relatively thin TGO layer (about 3.6 μm) which is in agreement with the measured parabolic constant for this BC. TGO is a pure alumina layer but many Ta–Ti rich particles can be observed at the TGO/BC interface. Further microstructural investigations are under way to elucidate the differences of TGO adhesion on NiPtAl and NiCoCrAlYTa bond coatings.

Fig. 5. SEM micrography of TBC48 after 80 cycles (BSE image).

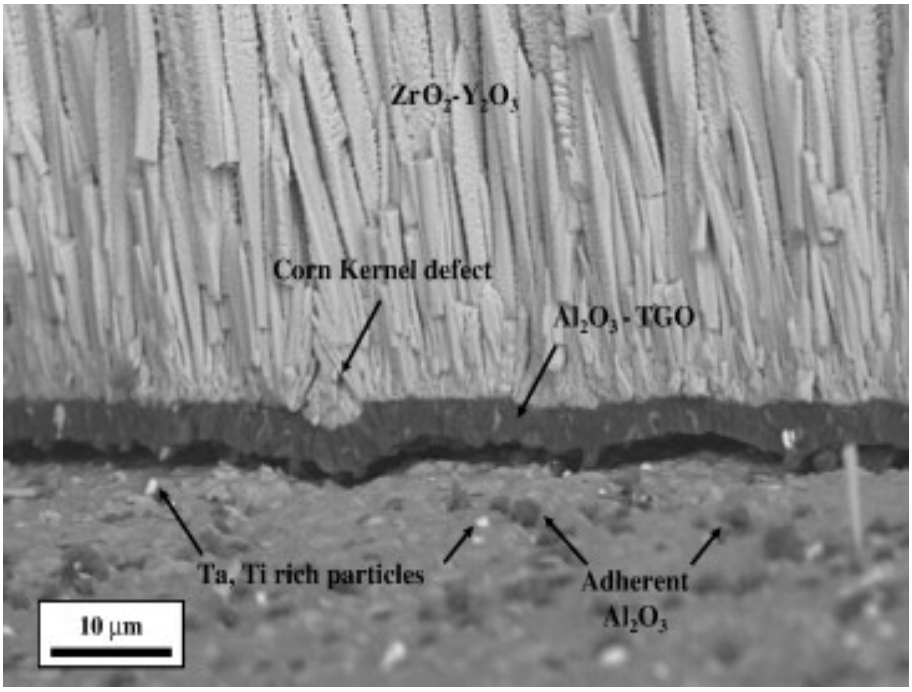

5. Conclusion

CTGA technique (apparatus and analysis) can be used for the automatic testing of the cyclic oxidation resistance of TBC systems. This technique has several advantages such as the precise determination of oxidation kinetics of the BC and the detection of very tiny spalling events of the zirconia top coating, with the determination of the temperature at which they occur. The better behavior of APVS NiPtAl over VPS NiCoCrAlYTa BC is confirmed at 1100 °C. This difference is not due to oxidation kinetics but to TGO adhesion. Comparative microstructural characterizations of the spalled samples will be necessary to elucidate this difference.

Acknowledgements

Snecma Service (A.Malié) and Turboméca-SAFRAN (F.Crabos) companies are gratefully acknowledged for the delivery of TBC samples, Turboméca and CNRS for financial support of A. Vande Put PhD.

References

D. Monceau and D. Poquillon, *Oxid. Met.* **61** (2004), p. 143.

D. Poquillon, D. Oquab, B. Viguier, F. Senocq and D. Monceau, *Mater. Sci. Eng.* **A38** (2004), p. 237.

A. Raffaitin, D. Monceau, E. Andrieu and F. Crabos, *Acta Mater.* **54** (2006), p. 4473.

R. Kartono, D. Monceau, D.J. Young, Scr. Mater. (submitted for publication).

R. Kartano et al. unpublished work.

D. Poquillon and D. Monceau, *Oxid. Met.* **59** (2003), p. 409.

J.L. Smialek, *Metall. Trans.* **A9** (1978), p. 309.

C.E. Lowell, C.A. Barrett, R.W. Palmer, J.V. Auping and H.B. Probst, *Oxid. Met.* **36** (1991), p. 81.

J.L. Smialek, *Acta Mater.* **51** (2003), p. 469.

A.G. Evans, D.R. Mumm, J.W. Hutchinson, G.H. Meier and F.S. Pettit, *Prog. Mater. Sci.* **46** (2001), p. 505.

D. Monceau, F. Crabos, A. Malié and B. Pieraggi, *Mat. Sci. Forum* (2001), p. 607.

J.C. Salabura and D. Monceau, *Mat. Sci. Forum* **461** (2004), p. 489.

D. Monceau and B. Pieraggi, *Oxid. Met.* **50** (1998), p. 477.

Original text : Elsevier.com